Theoretical and experimental investigations of rate coefficients of O(1 D) + CH 4 at low temperature

Qingyong Meng, Kevin Hickson, Kejie Shao, Jean-Christophe J.-C. Loison, Zhang Dong

Theoretical and Experimental Investigations of Rate Coefficients of O (^1D) + CH_4 at Low Temperature

Qingyong Meng,[1,2,*] Kevin M. Hickson,[3,†] Kejie Shao,[2] Jean-Christophe Loison,[3] and Dong H. Zhang[2,‡]

[1]*Department of Applied Chemistry, Northwestern Polytechnical University, Youyi West Road 127, 710072 Xi'an, China*

[2]*State Key Laboratory of Molecular Reaction Dynamics and Center for Theoretical and Computational Chemistry, Dalian Institute of Chemical Physics, Chinese Academy of Sciences, Zhongshan Road 457, 116023 Dalian, China*

[3]*CNRS UMR 5255, Institut des Sciences Moléculaires, Université de Bordeaux, Bâtiment A12, 351 Cours de la Libération, F-33400 Talence, France*

(Dated: September 19, 2016)

Abstract

Rate coefficients of the barrierless O (^1D) + CH_4 reaction are determined both theoretically and experimentally at 50 K - 296 K. For the calculations, ring polymer molecular dynamics (RPMD) simulations are performed on the basis of a new neural network potential energy surface (PES) in reactant asymptotic part. Only reactant asymptotic part PES is constructed because of its barrierless and exothermic properties. Experimentally, the reaction rate coefficients are measured using a supersonic flow reactor. Pulsed laser photolysis of O_3 molecules is used as the source of O (^1D) atoms, which are detected directly through vacuum ultraviolet laser induced fluorescence at 115 nm. The branching ratio for H atom production is measured by comparing the H atom yields of the O (^1D) + CH_4 and O (^1D) + H_2 reactions. At $T \geq 75$ K, good agreement between theoretical and experimental rate coefficients is found, while at 50 K, the larger difference is discussed in detail.

Keywords: *RPMD*; *NN PES*; *VUV-LIF*; *Rate coefficients*; *O (^1D) + CH_4*

*Electronic address: qingyong.meng@nwpu.edu.cn

†Electronic address: km.hickson@ism.u-bordeaux1.fr

‡Electronic address: zhangdh@dicp.ac.cn

I. INTRODUCTION

Due to its significance in both atmospheric and combustion chemistry, over the past decade the reaction of methane with O (^1D) has attracted great attention both experimentally [1–7] and theoretically [8–11], helping to unravel the dynamics and kinetics of this typical polyatomic complex-forming barrierless reaction. These studies [1–4, 8–10] have determined an approximately temperature-independent rate coefficient of $\sim$ 1.5 (unless otherwise specified, the rate is given in 10^{-10} cm$^3 \cdot$ s^{-1}) at the room temperature.

On the basis of a pseudo-triatomic three-dimensional (3D) ground-state ($^1A'$) potential energy surface (PES) [8], González *et al.* [8] and Ben Bouchrit *et al.* [10] reported rate coefficients of the O (^1D) + CH_4 $\rightarrow$ OH + CH_3 reaction from quasi-classical trajectory (QCT) [8] and time-independent quantum mechanical (TIQM) [10] reactive scattering calculations, respectively. They [8, 10] found (i) that quantum effects do not strongly affect the resulting rate coefficients and (ii) a rather good agreement between computations and experiments was obtained. Despite the existence of agreement at room temperature, it is still necessary to perform full dimensional (12D) quantum dynamics calculations because the CH_3 fragment was treated as a pseudo-triatom in previous calculations [8, 10]. Furthermore, below room temperature there are neither experimental measurements nor full dimensional quantum simulations available in the literature for this reaction.

Recently, Shao *et al.* [11] constructed a global full-dimensional ground-state PES of the O (^1D) + CH_4 system by permutationally invariant fitting to roughly 3.4×10^5 *ab initio* energy points with the maximum fitting error of dozen of meV. Since the fitting error of this global PIP PES is rather large, the dynamics simulations for the title reaction may only predict the rate coefficients with rather a large uncertainty. In this work, we re-construct a new, more accurate PES on the basis of the previous *ab initio* energy points [11]. Based on this new PES, ring-polymer molecular dynamics (RPMD) [12–16] simulations are performed to accurately and efficiently compute the rate coefficients. The RPMD method [12–16] exploits the isomorphism between the statistical properties of the quantum system and those of a fictitious ring polymer consisting of many replications of the original system, which are called beads, connected by harmonic springs. It has been shown that RPMD can be used to describe complex-forming reactions [17–19] and that RPMD is capable of providing fairly accurate estimates of the rate coefficients of gas phase polyatomic reactions involving methane [16, 20, 21].

Experimentally, the title reaction is studied over the range 50 K - 296 K using the contin-

uous supersonic flow method [22, 23] by following the kinetics of O (^1D) atom decay directly [24]. Temperature dependent branching ratios are also measured by following the production of H atoms. In this work, the temperature range of 50 K - 296 K is chosen because temperature in the Earth's atmosphere [25] is in the range of 100 K - 300 K.

This paper is organized as follows; in Section II, we will describe the experimental and theoretical methods. Sections III and IV presents the results and discussions, respectively. Finally, Section V concludes with a summary.

II. EXPERIMENTAL AND THEORETICAL METHODS

A. Experimental Method

All experiments are performed using a continuous supersonic flow apparatus which has been described in detail in previous work [19, 22–24, 26] at specified temperatures of 127 K, 75 K, and 50 K through the use of different argon based Laval nozzles, with experiments at 296 K being performed without a nozzle. As the non-reactive quenching of O (^1D) by N_2 is rapid at low temperature [24], it was impossible to use our nitrogen based nozzles for this investigation. The measured and calculated flow characteristics can be found in Table 1 of Grondin *et al.* [24].

O (^1D) atoms are created in the present experiments by the pulsed UV photo-dissociation of O_3 *in situ* in the supersonic flow at 266 nm with energies around 21 mJ. O_3 itself is produced by the continuous UV irradiation of O_2 as described by Grondin *et al.* [24]. The O (^1D) atoms are followed directly through resonant VUV-LIF using the 3s $^1D \rightarrow$ 2p ^1D transition at 115.215 nm. Tunable radiation at this wavelength is produced by frequency doubling 691.29 nm light before focusing the doubled output into a cell containing 100 Torr of Xe and 230 Torr of Ar for third harmonic generation. For the branching ratio measurements leading to H and OH products, tunable light at and around the H (^2S) Lyman α transition at 121.567 nm is generated by a similar procedure to the one described above for the detection of O (^1D) atoms, using a fundamental wavelength of 729.4 nm and 210 Torr of Kr and 540 Torr of Ar in the tripling cell. The VUV light generated in this way is collimated by a magnesium fluoride lens at the cell exit, with the tripling cell situated perpendicular to both the observation axis and the supersonic flow. Fluorescence from cold atoms within the supersonic flow is collected perpendicular to the supersonic flow axis and the tripling cell by a solar blind photomultiplier tube (PMT) which is isolated from the flow reactor

by a lithium fluoride (LiF) window. The evacuated region between the PMT and the LiF window contained an LiF lens to focus the atomic fluorescence emission onto the PMT photocathode. The PMT output is fed into a boxcar integrator coupled to a computer for signal acquisition. O (^1D) and H (^2S) VUV-LIF signals are recorded as a function of time between photolysis and probe lasers with the timing being controlled by a delay generator. 30 laser shots are averaged at each time point, with each kinetic decay consisting of at least 40 intervals. To establish the baseline signal, several time points are recorded with the probe laser firing prior to the photolysis laser.

The gases used in the experiments (Ar 99.999%, O_2 99.999%, Xe 99.998%, CH_4 99.9995%, H_2 99.9995%) are flowed directly from cylinders into calibrated mass flow controllers, allowing us to calculate the reagent and precursor concentrations from their flow ratios using the calculated supersonic flow densities.

B. Theoretical Method

In this work, the rate coefficients of the O (^1D) + CH_4 reaction are computed based on a local PES in the reactant asymptotic part because of its barrierless and exothermic properties [8, 9, 11]. In order to construct this local PES, the fundamental invariant neural network (FI-NN) fitting method [27] is used to fit a 81-15-40-1 NN function with 1911 parameters to a total of 36690 *ab initio* points, which were computed at the MRCI+Q/aug-cc-pVTZ level [11]. In the NN function, the activation function of $\frac{x}{\sqrt{1+x^2}}$ is used. Among these *ab initio* points, 90% are used as the training set, while the other 10% are used as the validating set. The training and validating deviations of the NN PES are 0.208 and 0.239 meV, respectively.

Since the RPMD method has been well reviewed elsewhere [12–16, 28], only brief notes are given here. Consider an N-atomic (*i.e.* $3N$-dimensional) system with momenta $\mathbf{p} = \{\mathbf{p}_i\}_{i=1}^N$, positions $\mathbf{r} = \{\mathbf{r}_i\}_{i=1}^N$, and potential energy $V(\mathbf{r}_1, \cdots, \mathbf{r}_N)$. The RPMD Hamiltonian is proved [12, 13] in the following $(3N \times n)$-dimensional form

$$H_n(\mathbf{p}, \mathbf{r}) = \sum_{j=1}^{n} \left\{ \sum_{i=1}^{N} \left(\frac{|\mathbf{p}_i^{(j)}|^2}{2m_i} + \frac{1}{2} m_i \omega_n^2 \left| \mathbf{r}_i^{(j)} - \mathbf{r}_i^{(j-1)} \right|^2 \right) + V(\mathbf{r}_1^{(j)}, \cdots, \mathbf{r}_N^{(j)}) \right\}, \tag{1}$$

where $\omega_n = (\beta_n \hbar)^{-1}$, $\beta_n = \beta/n$, $\beta = 1/(k_B T)$, and $\mathbf{r}_i^{(0)} = \mathbf{r}_i^{(n)}$.

Based on equation (1), extensive classical molecular-dynamics (MD) simulations are performed to compute the RPMD rate coefficients [14–16], which can be written as the Bennett-Chandler factorization [29], $k_{\mathrm{RPMD}}^{(n)}(T) = k_{QTST}(s_0, T) \cdot \kappa^{(n)}(t_p, T, s^{\ddagger}) \cdot \exp\left(-\beta \Delta W^{(n)}\right)$. Here $k_{QTST}(s_0, T)$ is the

surface area of a sphere with large enough radius times the thermally averaged flux of reactants entering this sphere, $\kappa^{(n)}$ is the transmission coefficient at the peak position of the free-energy curve, and $\Delta W^{(n)}$ is the free-energy barrier. s is the scaled reaction coordinate, where $s_0 = 0.0$ and $s = 1.0$ represent reactant and product asymptotic groups, respectively. It is worth noting that there exists $\Delta W^{(n)}$ for this barrierless reaction. We shall return to this point later.

As given above, only intermediate-forming part of the reaction coordinate, $s \in [-0.05, 0.26]$, is involved in computing $\Delta W^{(n)}$. This part of s is divided into 107 windows, called umbrella-sampling geometries. Within each window, extensive RPMD simulations are performed to obtain the mean force $\partial W/\partial s$ and then $\Delta W^{(n)}$ is determined by numerical integration. To do this, the RPMD system is first equilibrated for 20 ps, followed by a production run of 100 ps. Next, the transmission coefficient $\kappa^{(n)}$ is computed by first equilibrating for 20 ps, and then sampling the initial configurations once every 2 ps to serve as the initial positions for 100 child trajectories with $t_p = 7$ ps. Here a total of 2.0×10^5 trajectories are evolved for $\kappa^{(n)}$. All of the RPMD simulations are carried out using the modified version of the RPMDrate package [30].

III. RESULTS

A. Experimental Measurements

As there exist two main product channels for the O (^1D) + CH_4 reaction, leading to OH + CH_3 and H + CH_2OH/CH_3O products, it is important to quantify the contribution of these pathways. By comparing the amplitude of the H atom signal from the O (^1D) + CH_4 reaction versus the one obtained from a reference process, the O (^1D) + H_2 reaction recorded at the same time, (assuming that this reaction produces atomic hydrogen with a 100% yield) it was possible to determine the sum of the H atom branching channels at a given temperature. In the left panel of Figure 1 we show the measured H atom fluorescence intensity as a function of time for both the target O (^1D) + CH_4 and reference O (^1D) + H_2 reactions at 50 K. At least seven pairs of decays similar to the ones shown are recorded at each temperature, to minimize potential experimental errors. At 50 K and 296 K, mean values of 0.20 ± 0.01 and 0.21 ± 0.01 respectively are obtained with these statistical errors cited at the level of one standard deviation. This result is in excellent agreement with the previous crossed molecular beam experimental determination of the OH + CH_3 product channel branching ratio of 0.77 at higher energy [31]. Moreover, on the basis of the PIP PES, QCT

simulations [11] also predicted a branching ratio of 0.8 for this channel.

Example traces of the O (^1D) VUV-LIF signal intensity as a function of time recorded at 50 K with the carrier gas Ar alone, and with added CH_4 are shown in the right panel of Figure 1. It can be seen that O (^1D) is more efficiently removed when CH_4 is present in the supersonic flow, although collisions with Ar also lead to its rapid loss through quenching to the ground state O (^3P). Nevertheless, [Ar] is fixed for any series of measurements, so that this process represents a constant pseudo-first order loss for O (^1D). Methane is added as the excess reagent, so that simple exponential fits to these temporal profiles allowed us to determine the total pseudo-first-order rate coefficients for O (^1D) loss from the time constant. Other potential loss processes for O (^1D) atoms including quenching by O_2 and O_3, and loss through diffusion are all negligibly small when compared to the quenching induced by the carrier gas Ar and by the reactive losses with CH_4. A discussion of these additional losses can be found in Grondin *et al.* [24]. To determine the second-order rate coefficients at a specified temperature, the excess CH_4 concentrations are varied and the resulting pseudo-first-order rate coefficients are plotted against the corresponding CH_4 concentration as shown in Figure 2. The gradient of the straight line fit to these data (weighted by the calculated uncertainties of fits to the individual decay profiles) yields the final rate coefficient. The y-axis intercept value of these plots is large, corresponding to the relaxation of O (^1D) atoms mostly through collisions with the carrier gas Ar. We will discuss the temperature-dependent rate coefficients after showing the theoretical calculations. In Table I, the number of individual measurements and the range of CH_4 concentrations (in 10^{14} cm^{-3}) used in measurements are also given.

B. Theoretical Calculations

In order to accurately compute the overall rate coefficients, let us first consider the extended Hinshelwood type mechanism of the O (^1D) + CH_4 reaction, $A+B \underset{k_{-a}}{\overset{k_a}{\rightleftharpoons}} C \xrightarrow{k_r} P$, where A and B are reactants, C is intermediate, and P is product. Applying the steady state approximation to the intermediate complex C, it is easy to obtain the overall rate coefficient in the form $k = \frac{k_r k_a}{k_{-a}+k_r} = \frac{k_a}{k_{-a}/k_r+1}$, where k_a can be computed by RPMD simulations based on a local PES of reactant asymptotic part and the chemical activation ratio k_{-a}/k_r can be estimated by the free-energy difference of the reactants and products, $\Delta_r W$. Because of the large value of $|\Delta_r W|$ for the title reaction (larger than 1.5 eV), k_{-a}/k_r must be very close to zero. Indeed, the RPMD simulations on the global PIP PES

[11] predict that $k_{-a}/k_r \sim 0$ and hence $k \simeq k_a$, which implies that the Hinshelwood type mechanism is a good approximation. Therefore to compute k_a, we construct the local PES using the NN fitting method and the previous MRCI+Q energy database [11]. As shown in Figure 3, this local NN PES shows a very low fitting error (less than 1.0 meV) over the energy range of 0.0 - 1.5 eV, which implies that it is highly accurate.

Let us turn to the RPMD simulations. To determine the number of beads n in computing $\Delta W^{(n)}$, RPMD simulations with $n = 1$, $n = 4$, and $n = 8$ are performed at 75 K and 100 K. At 75 K the free-energy barriers from $n = 1$, $n = 4$, and $n = 8$ are 1.8, 1.5, and 1.6 meV, respectively. At 100 K the free-energy barriers from $n = 1$, $n = 4$, and $n = 8$ are 2.6, 2.1, and 2.5 meV, respectively. The errors of $\exp(-\beta\Delta W^{(n)}(T))$ associated with n are then smaller than 6%. These free energy results clearly show that one can use $n = 4$ to compute $\Delta W^{(n)}$. Similarly, $n = 1$ is found to be enough to compute $\kappa^{(n)}$. The convergence of small number of beads should be caused by the small zero point energy (ZPE) differnece (3.16 kcal/mol) [11] between the reactants and the complex. Moreover, the small number of beads for both $\Delta W^{(n)}$ and $\kappa^{(n)}$ implies that quantum effects do not strongly affect the rate coefficients, in a similar manner to previous 3D TIQM [10] simulations.

Next, after inspecting the convergence, the temperature-dependent $\Delta W^{(n)}$ are computed and resulting free-energy curves are given in the left panel of Figure 4. Although O (^1D) + CH_4 is potential-energy barrierless, it can be found that the RPMD free energy curves do indeed display barriers. This is because the decrease in enthalpy from reactants to the peak of free-energy is somewhat compensated by a decrease in entropy, which clearly indicates the competition between decrease of potential energy and damping from unreactive coordinates of the system. Curves of transmission coefficients versus evolution time t are given in the right panel of Figure 4, where one can find the $\kappa^{(n)}$ curves oscillate with a frequency of approximately 10 fs. These oscillations may be associated with stretching modes (3130 and 3196 cm^{-1} [11]) of the C-H bonds in methane, whose periods are roughly 10 fs.

C. Rate Coefficients

The present VUV-LIF and RPMD rate coefficients, together with previous computational [8–11] and experimental [1–7] results are given in Table I. For clarity, in Figure 5 we show the rate coefficients as a function of temperature.

At 296 K the present VUV-LIF result of 1.65 ± 0.17 is close to previous experimental results

[1–4] as well as the IUPAC recommended value of 1.50 ± 0.36 [5–7]. The relative differences are smaller than 10%, which implies that the present VUV-LIF measurements are accurate. It should be noted at this point that the rate coefficient values measured in this study, along side those of Blitz *et al.* [2] were the only ones to be obtained using direct detection of O (^1D) atoms. All other previous studies used a range of indirect detection methods to follow the progress of the O (^1D) + CH_4 reaction.

Now, let us compare the RPMD rate coefficients with the previous QCT and [8] and TIQM [10] results. As shown in Table I, the previous QCT results [8] at 300 K and 200 K are given to compare with the RPMD ones at 296 K and 210 K. Although there is temperature difference (smaller than 10 K), good agreement between RPMD and QCT [8] can be found. The relative differences are smaller than 20%. Next, turning to the TIQM results, since TIQM calculations were performed for the OH + CH_3 channel only, they are first scaled by a branching ratio of 0.78, which was previously determined [10]. After scaling the TIQM rate coefficients, reasonably good agreement between RPMD and TIQM [10] results is found. The relative differences are smaller than 28%, except for the one at 50 K (roughly 37%). These differences may arise from the following three points. First, the reduced dimensional (3D) PES [10] was constructed by the UMP2/6-311G(2df,2pd) energy points, while the present full dimensional (12D) PES is constructed at the higher MRCI+Q/aug-cc-pVTZ level. Second, potential energy functions and fitting errors of these two PESs may influence the final rate results. Finally, the 3D TIQM calculations [10] may lose dynamics information, such as contributions of the umbrella vibration of the CH_3 fragment and symmetric/asymmetric stretching vibrations of CH_4, even though previous work has shown these contributions to be small [10].

Finally, let us compare the present VUV-LIF and RPMD rate coefficients. At 75 K, 127 K, and 296 K, good agreement between RPMD and VUV-LIF results is found with relative differences being smaller than roughly 20%. At 50 K, however, the relative difference between RPMD and VUV-LIF results is 42%. This larger relative difference could arise from (i) contributions of excited state PESs of the O (^1D) + CH_4 system, (ii) an absence of long range (LR) interactions between O (^1D) and CH_4, and (iii) errors in *ab initio* calculations and construction of the PES. Now, let us discuss these points in detail.

IV. DISCUSSIONS

It has been found that the contribution of excited states, in particular the $^1A''$ state of O (^1D), may play a non-negligible role in the reaction. Through their CASPT2 and CASSCF calculations, Hernando *et al.* [9] expected a significant contribution of the excited 2 ^1A PES to the O (^1D) + CH_4 reaction. Recently, two of us (K.M.H. and J.-C.L.) found opposite temperature dependence for reaction over the $^1A'$ and $^1A''$ PESs of the C (^1D) + H_2 system [19]. The RPMD rate for the 1 ^1A ($^1A'$) PES was found to increase with temperature, while that for 2 ^1A ($^1A''$) decreases with temperature. The net effect was seen to be a very slight increase in the total rate coefficient [19]. The 2 ^1A ($^1A''$) PES of the O (^1D) + CH_4 reaction could play the same role as in the case of C (^1D) + H_2. However, this is still an open question since the excited-state PESs of the O (^1D) + CH_4 system are not currently available.

On the other hand, the rather small RPMD $\kappa^{(n)}$ values might cause the rather small rate coefficient at 50 K. As shown in the right panel of Figure 4, at $T > 75$ K the $\kappa^{(n)}$ values in the plateau region decrease with increasing temperature. However, the situation is changed at 50 K, where the $\kappa^{(n)}$(50 K) value is smaller than expected. Adding a perturbated LR attractive potential, we might expect that the value of $\kappa^{(n)}$(50 K) increases. Consequently, the computed rate coefficient at 50 K increases.

Now let us turn to the LR potential itself. Adding the LR interaction model of $\alpha_1 R^{-3} - \alpha_2 R^{-4}$ into the PES of the $D^+ + H_2$ system, Lara *et al.* [32] reported good agreement between theoretical and experimental temperature-independent rate coefficients at 10 K - 90 K [32]. In their LR potential model, the dominant contributions involve the charge-quadrupole interaction R^{-3} and the charge-induced dipole R^{-4}. Obviously, this LR potential is too attractive for the present radical-molecule system. We might expect a $\propto R^{-6}$ LR model and hence the rate coefficients more slowly approach to zero as $T \rightarrow 0$ than those shown in Figure 5. However, the application of the LR potential model for the O (^1D) + CH_4 system is still an open question.

Finally, the errors in constructing the PES may be another reason. In the present work, a set of MRCI+Q/aug-cc-pVTZ energy points [11] are used to construct the present NN PES. Although the systematic and random errors are small as shown in Figure 3, errors may still be introduced through the initial MRCI+Q calculations and constructions. At temperatures as low as 50 K, since the free-energy barriers are smaller than 1.5 meV, these PES errors may influence the resulting free-energy barrier and hence the rate coefficients. However, it will be difficult to further improve

the present RPMD results because the present PES error of roughly 1 meV is already very small.

V. CONCLUSIONS

In summary, we determine rate coefficients for the barrierless O (^1D) + CH_4 reaction at low temperatures (50 K - 296 K) both theoretically and experimentally. On the basis of the present local and accurate NN PES, extensive RPMD calculations are performed, predicting similar rate coefficients and a similar temperature-dependence to the experimental VUV-LIF rate coefficients. Moreover, the fact that a small number of beads can approach convergence clearly implies that quantum effects do not strongly affect the rate coefficient values, a result which was also found by previous TIQM calculations [10]. Experimentally, the rate coefficients at 50 K, 75 K, 127 K, and 296 K are measured using a supersonic flow reactor, where the pulsed laser photolysis of O_3 molecules is used as the source of O (^1D) atoms. During the measurements, O (^1D) is detected directly by VUV-LIF at 115 nm. A comparison of the present VUV-LIF rate coefficients with the RPMD ones, leads to rather large difference between the experimental and theoretical rate coefficients at 50 K. This may be due to several reasons, including possible contributions of excited state surfaces and the LR interaction. Furthermore, errors in the *ab initio* calculations and/or construction of the PES may also influence the resulting rate coefficients. Therefore, further work is required to improve the calculated rate coefficients at $T < 75$ K. However, since the atmosphere temperature in the Earth is in the range of 100 K - 300 K [25], the present calculations and experiments provide very useful references for atmospheric chemistry.

Acknowledgments

K.M.H. and J.-C.L. thank the CNRS programs PCMI and PNP for their support. Q.M., K.S., and D.H.Z. thank Ministry of Science and Technology of P. R. China (Grant No. 2013CB834601), National Natural Science Foundation of China (Grant Nos. 21433009 and 21503214), and Chinese Academy of Sciences (Grant No. XDB17010200). Q.M. also acknowledges the start-up fund from Northwestern Polytechnical University. Q.M. wishes to thank Dr. B. Fu for discussing on the dynamics of the O (^1D) + CH_4 system. We thank Prof. Dr. P. Honvault for providing their 3D

TIQM results.

---

[1] S. T. Amimoto, A. P. Force, J. R. G. Gulotty, and J. R. Wiesenfeld. *J. Chem. Phys.* **871** (1979), 3640–3647.

[2] M. A. Blitz, T. J. Dillon, D. E. Heard, M. J. Pilling, and I. D. Trought. *Phys. Chem. Chem. Phys.* **6** (2004), 2162–2171.

[3] T. J. Dillon, A. Horowitz, and J. N. Crowley. *Chem. Phys. Lett.* **443** (2007), 12 – 16.

[4] S. Vranckx, J. Peeters, and S. Carl. *Phys. Chem. Chem. Phys.* **10** (2008), 5714–5722.

[5] R. Atkinson, D. L. Baulch, R. A. Cox, R. F. Hampson, J. A. Kerr, M. J. Rossi, and J. Troe. *J. Phys. Chem. Ref. Data* **28** (1999), 191–393.

[6] R. Atkinson, D. L. Baulch, R. A. Cox, J. N. Crowley, R. F. Hampson, R. G. Hynes, M. E. Jenkin, M. J. Rossi, and J. Troe. *Atmos. Chem. Phys.* **6** (2006), 3625–4055.

[7] S. P. Sander, A. R. Ravishankara, D. M. Golden, C. E. Kolb, M. J. Kurylo, M. J. Molina, G. K. Moortgat, B. J. Finlayson-Pitts, P. H. Wine, R. E. Huie, and V. L. Orkin. *Chemical Kinetics and Photochemical Data for Use in Atmospheric Studies. Evaluation No. 15*. JPL publication, Jet Propulsion Laboratory, Pasadena, 2006.

[8] M. M. González, J. Hernando, M. P. Puyuelo, and R. Sayós. *J. Chem. Phys.* **113** (2000), 6748–6759.

[9] J. Hernando, J. Millán, R. Sayós, and M. González. *J. Chem. Phys.* **119** (2003), 9504–9512.

[10] R. Ben Bouchrit, M. Jorfi, D. Ben Abdallah, N. Jaidane, M. González, B. Bussery-Honvault, and P. Honvault. *J. Chem. Phys.* **140** (2014), 244315.

[11] K. Shao, B. Fu, and D. H. Zhang. *Phys. Chem. Chem. Phys.* **17** (2015), 24098–24107.

[12] I. R. Craig and D. E. Manolopoulos. *J. Chem. Phys.* **122** (2005), 084106.

[13] I. R. Craig and D. E. Manolopoulos. *J. Chem. Phys.* **123** (2005), 034102.

[14] R. Collepardo-Guevara, Y. V. Suleimanov, and D. E. Manolopoulos. *J. Chem. Phys.* **130** (2009), 174713.

[15] R. Collepardo-Guevara, Y. V. Suleimanov, and D. E. Manolopoulos. *J. Chem. Phys.* **133** (2010), 049902.

[16] Y. V. Suleimanov, R. Collepardo-Guevara, and D. E. Manolopoulos. *J. Chem. Phys.* **134** (2011), 044131.

[17] Y. Li, Y. V. Suleimanov, and H. Guo. *J. Phys. Chem. Lett.* **5** (2014), 700 – 705.

[18] Y. V. Suleimanov, W. J. Kong, H. Guo, and W. H. Green. *J. Chem. Phys.* **141** (2014), 244103.

[19] K. M. Hickson, J.-C. Loison, H. Guo, and Y. V. Suleimanov. *J. Phys. Chem. Lett.* **6** (2015), 4194–4199.

[20] Q. Meng, J. Chen, and D. H. Zhang. *J. Chem. Phys.* **143** (2015), 101102.

[21] Q. Meng, J. Chen, and D. H. Zhang. *J. Chem. Phys.* **144** (2016), 154312.

[22] B. R. Rowe, G. Dupeyrat, J. B. Marquette, and P. Gaucherel. *J. Chem. Phys.* **80** (1984), 4915–4921.

[23] N. Daugey, P. Caubet, A. Bergeat, M. Costes, and K. M. Hickson. *Phys. Chem. Chem. Phys.* **10** (2008), 729–737.

[24] R. Grondin, J.-C. Loison, and K. M. Hickson. *J. Phys. Chem. A* **120**, 27 (2016), 4838–4844.

[25] E. L. Fleming, S. Chandra, J. J. Barnett, and M. Corney. *Adv. Space Res.* **10** (1990), 11 – 59.

[26] R. J. Shannon, C. Cossou, J.-C. Loison, P. Caubet, N. Balucani, P. W. Seakins, V. Wakelam, and K. M. Hickson. *RSC Adv.* **4** (2014), 26342–26353.

[27] K. Shao, J. Chen, Z. Zhao, and D. H. Zhang. *J. Chem. Phys.* **145** (2016), 071101.

[28] I. R. Craig and D. E. Manolopoulos. *J. Chem. Phys.* **121** (2004), 3368.

[29] C. H. Bennett. Molecular dynamics and transition state theory: The simulation of infrequent events. In *Algorithms for Chemical Computations, ACS Symposium Series Volume 46*, R. E. Christoffersen, Ed. American Chemical Society, Washington, D. C., 1977, pp. 63 – 97.

[30] Y. V. Suleimanov, J. W. Allen, and W. H. Green. *Computer Phys. Comm.* **184** (2013), 833 – 840.

[31] J. J. Lin, J. Shu, Y. T. Lee, and X. Yang. *J. Chem. Phys.* **113** (2000), 5287–5301.

[32] M. Lara, P. G. Jambrina, F. J. Aoiz, and J.-M. Launay. *J. Chem. Phys.* **143** (2015), 204305.

TABLE I: Summary of the present VUV-LIF rate coefficients (given in $cm^3 \cdot s^{-1}$) of the O (^1D) + CH_4 reaction, together with the RPMD ones. The first column gives the temperature in Kelvin. The second column gives number of individual measurements. The third column gives the range of concentrations (in 10^{14} cm^{-3}) of CH_4 used in the measurements. The rightmost two columns give the relative differences (in percentage) between (i) the present VUV-LIF and RPMD results, and (ii) the present RPMD and previous 3D TIQM [10] results. The other columns present the rate coefficients. For clarity, the rate coefficients as a function of temperature are shown in Figure 5.

T/K [a]	$N_{measur.}$	[CH_4]	Rate coefficient			Rel. Diff.	
			VUV-LIF [a,b]	RPMD [b]	Previous	RPMD/VUV-LIF	RPMD/TIQM (RPMD/QCT)
296	40	0 ~ 13	$(1.65 \pm 0.17) \times 10^{-10}$	1.84×10^{-10}	$(1.50 \pm 0.36) \times 10^{-10}$ [c]	11.5%	−18.6% (20.3%)
					$(1.93 \pm 0.14) \times 10^{-10}$ [d]		
					$(1.70 \pm 0.30) \times 10^{-10}$ [e]		
					2.26×10^{-10} [f]		
					1.53×10^{-10} [g]		
210	—	—	—	1.61×10^{-10}	2.15×10^{-10} [f]	—	−25.1% (−4.7%)
					1.69×10^{-10} [g]		
175	—	—	—	1.61×10^{-10}	2.06×10^{-10} [f]	—	−21.8%
127 ± 2	34	0 ~ 11	$(1.44 \pm 0.15) \times 10^{-10}$	1.52×10^{-10}	1.88×10^{-10} [f]	5.6%	−19.1%
100	—	—	—	1.34×10^{-10}	1.73×10^{-10} [f]	—	−22.5%
75 ± 2	42	0 ~ 6	$(1.38 \pm 0.16) \times 10^{-10}$	1.10×10^{-10}	1.53×10^{-10} [f]	−20.3%	−28.1%
50 ± 1	41	0 ~ 8	$(1.38 \pm 0.15) \times 10^{-10}$	7.99×10^{-11}	1.25×10^{-10} [f]	−42.1%	−36.8%

[a] Uncertainties on the temperatures represent the statistical (1σ) errors obtained from Pitot tube measurements of the impact pressure. Uncertainties on the measured rate coefficients represent the combined statistical (1σ) and estimated systematic (10%) errors.

[b] Present work.

[c] IUPAC recommended value [5–7].

[d] Chemiluminescence measurements of Vranckx *et al.* [4].

[e] PLP-PLIF value by Dillon *et al.* [3].

[f] TIQM values by Ben Bouchrit *et al.* [10].

[g] The QCT values of González *et al.* [8] at 200 K and 300 K are shown.

Figure Captions

Figure 1: VUV-LIF intensity as a function of time at 50 K for H (^2S) atom formation (left panel) and decay of O (^1D) atoms (right panel). In the left panel, the blue open circles represent the H-atom signal from the O (^1D) + CH_4 reaction with [CH_4] = 5.7×10^{14} cm^{-3}, while red solid circles represent the H-atom signal from the O (^1D) + H_2 reference reaction with [H_2] = 5.7×10^{14} cm^{-3}. In the right panel, the blue open circles represent the O-atom signal with no added methane, where O (^1D) decay is almost entirely due to to quenching with the carrier gas Ar. The red filled circles represent the O-atom signal with [CH_4] = 8.4×10^{14} cm^{-3}. In both sub-figures, the blue (or red) solid lines are exponential fits to the corresponding data points.

Figure 2: Pseudo-first-order rate constants for the O (^1D) + CH_4 reaction as a function of the methane concentration. A weighted linear least squares fit yields the second-order rate coefficient. Red open circles represent VUV-LIF measurements of the rate coefficient at 296 K, while blue filled circles represent those recorded at 50 K. The error bars reflect the statistical uncertainties at the level of a single standard deviation obtained by fitting to temporal profiles such as those shown in Figure 1.

Figure 3: The NN Fitting errors of energy points as a function of the corresponding *ab initio* potential energies. These energy points are used to construct the present local NN PES for the O (^1D) + CH_4 asymptotic part. All energies are relative to the reactant asymptote.

Figure 4: Comparison of the RPMD free-energy curves (left panel) and transmission coefficient curves (right panel) for O (^1D) + CH_4 at 50 K (black), 75 K (red), 100 K (green), 127 K (blue), 175 K (yellow), 210 K (brown), and 296 K (violet). The free energy in the left panel is drawn as a function of scaled reaction coordinate s, while the transmission coefficient in the right panel is drawn as a function of evolution time (in fs) of child trajectory.

Figure 5: Experimental and theoretical rate coefficients (in cm$^3 \cdot$s^{-1}) of the O (^1D) + CH_4 reaction as a function of the temperature (in Kelvin). The black "+" and red "$*$" symbols represent present RPMD and VUV-LIF rate coefficients, respectively. The other symbols with error bars repre-

sent previous experimental results [1–7]. Finally, the maroon "×" and the magenta "A" symbols represent previous QCT [8] and TIQM [10] results, respectively.

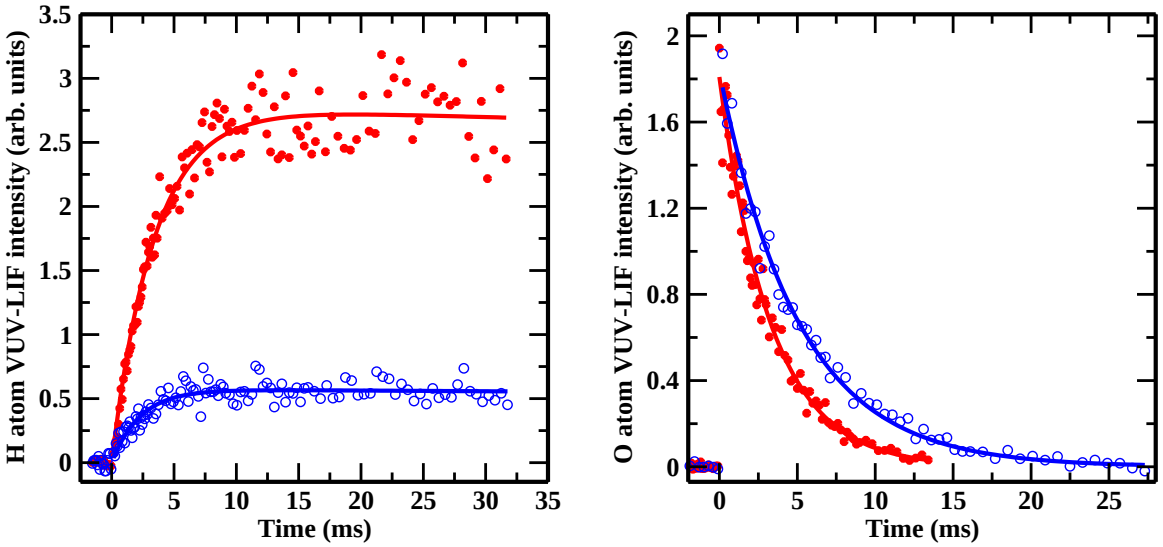

FIG. 1: RPMD, PIP PES, O + CH4

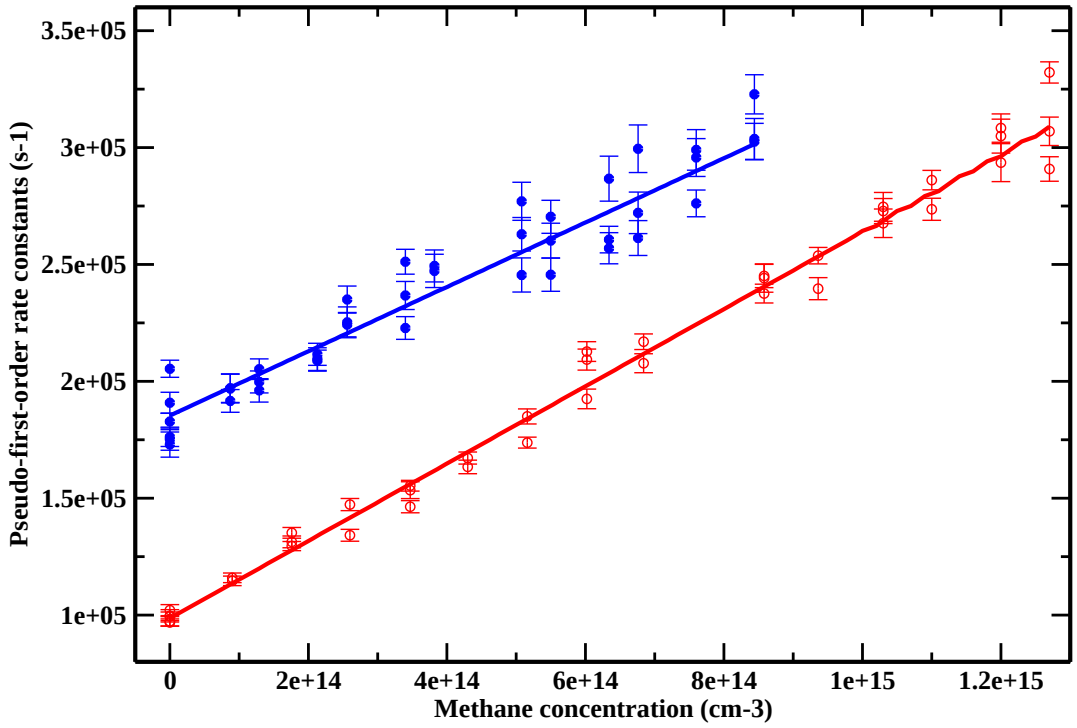

FIG. 2: RPMD, PIP PES, O + CH4

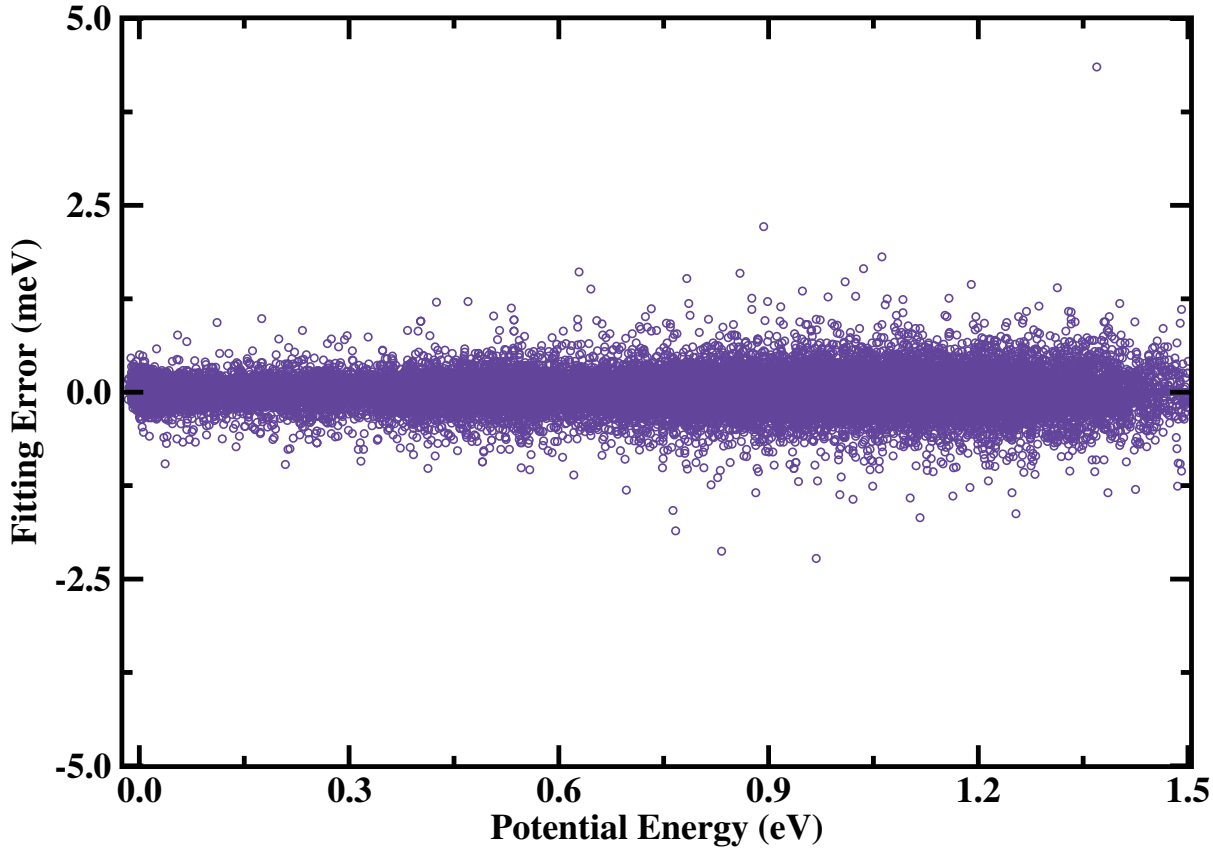

FIG. 3: RPMD, PIP PES, O + CH4

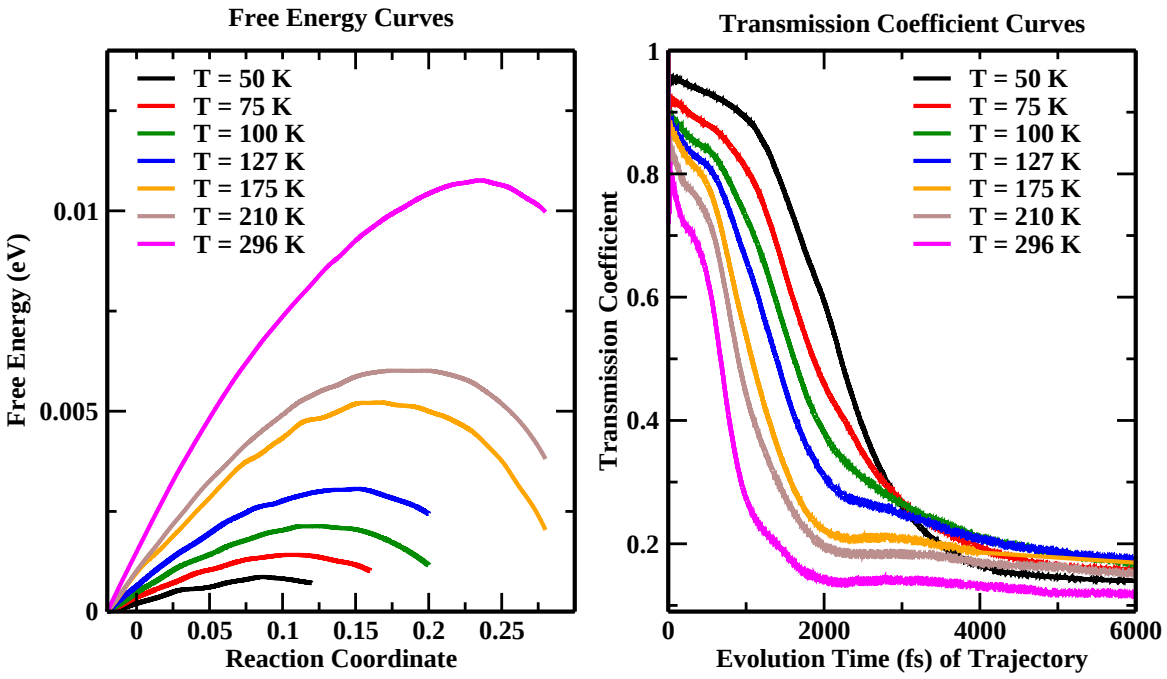

FIG. 4: RPMD, PIP PES, O + CH4

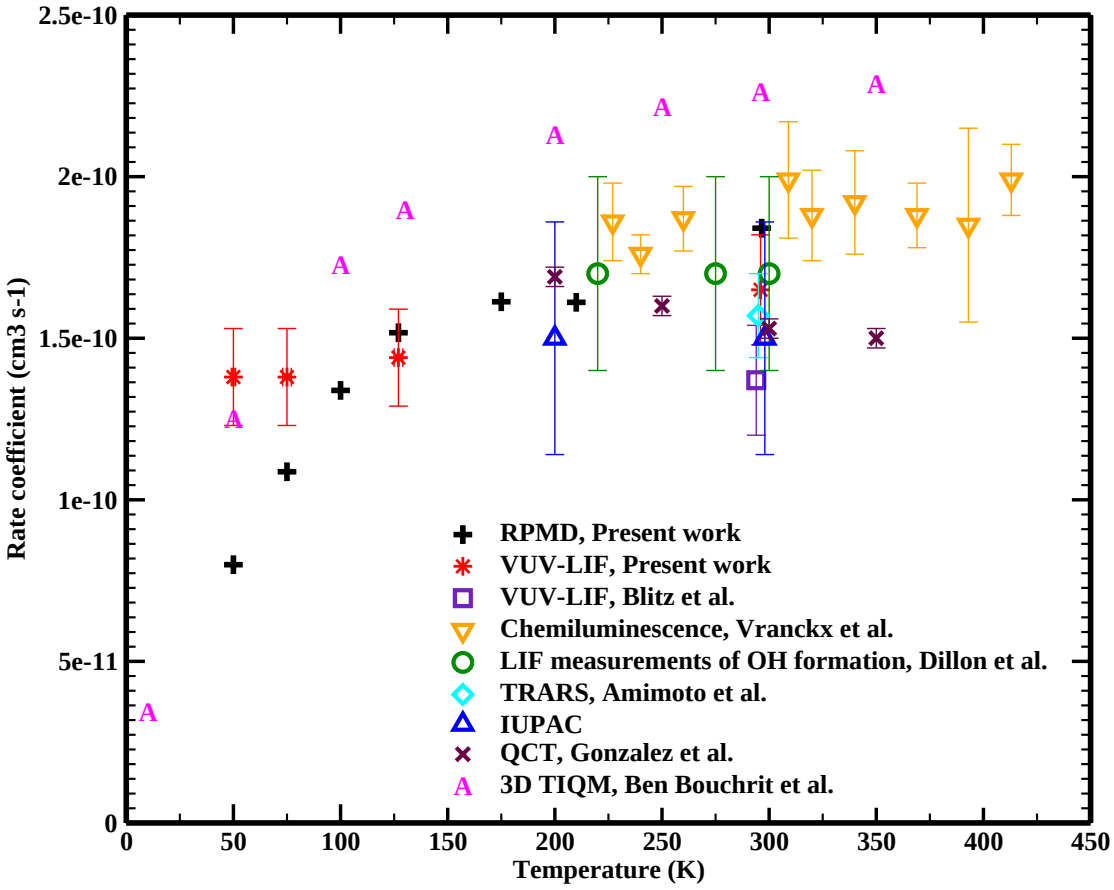

FIG. 5: RPMD, PIP PES, O + CH4

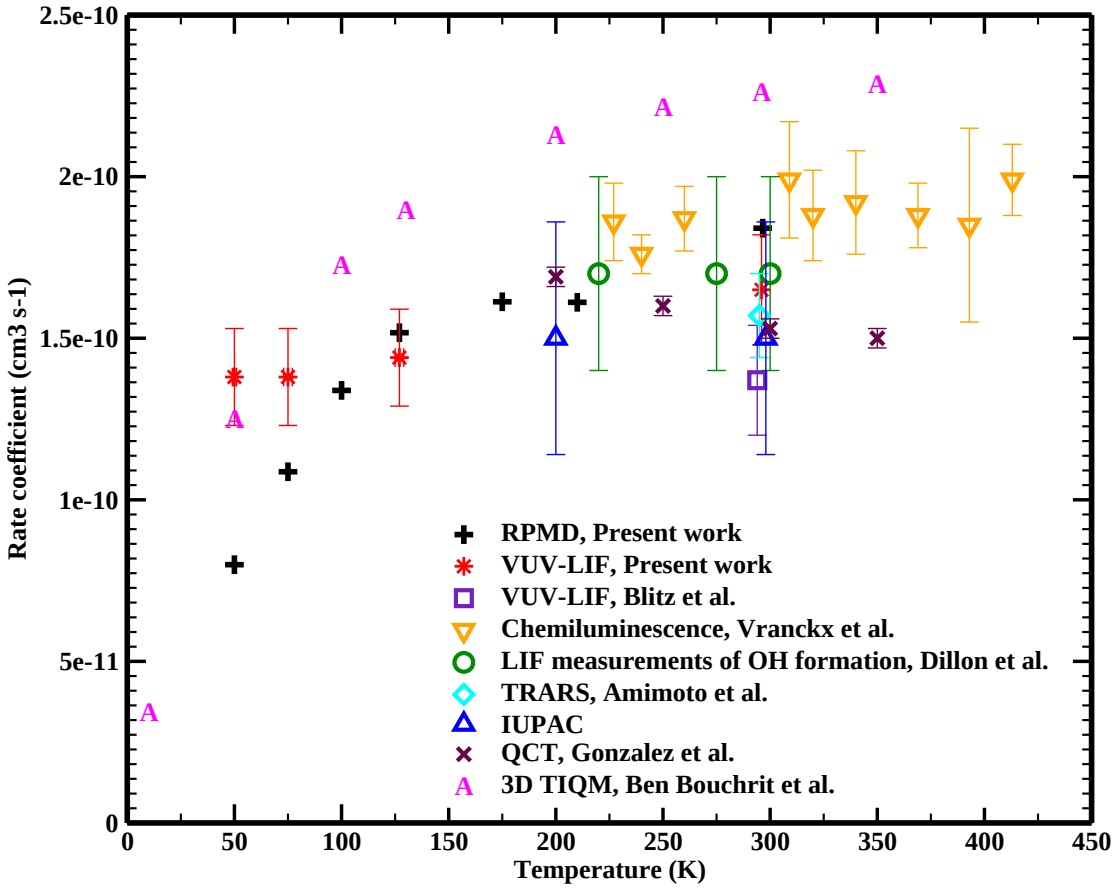

Table of Contents (TOC) Graphic

Abstract: The O (^1D) + CH_4 rates from RPMD and VUV-LIF are close to each other in the temperature range of atmosphere.